

DELAUNAY BIFILTRATIONS OF FUNCTIONS ON POINT CLOUDS

ÁNGEL JAVIER ALONSO, MICHAEL KERBER, TUNG LAM, AND MICHAEL LESNICK

ABSTRACT. The Delaunay filtration $\mathcal{D}_\bullet(X)$ of a point cloud $X \subset \mathbb{R}^d$ is a central tool of computational topology. Its use is justified by the topological equivalence of $\mathcal{D}_\bullet(X)$ and the offset (i.e., union-of-balls) filtration of X . Given a function $\gamma : X \rightarrow \mathbb{R}$, we introduce a Delaunay bifiltration $\mathcal{DC}_\bullet(\gamma)$ that satisfies an analogous topological equivalence, ensuring that $\mathcal{DC}_\bullet(\gamma)$ topologically encodes the offset filtrations of all sublevel sets of γ , as well as the topological relations between them. $\mathcal{DC}_\bullet(\gamma)$ is of size $O(|X|^{\lceil \frac{d+1}{2} \rceil})$, which for d odd matches the worst-case size of $\mathcal{D}_\bullet(X)$. Adapting the Bowyer-Watson algorithm for computing Delaunay triangulations, we give a simple, practical algorithm to compute $\mathcal{DC}_\bullet(\gamma)$ in time $O(|X|^{\lceil \frac{d}{2} \rceil + 1})$. Our implementation, based on CGAL, computes $\mathcal{DC}_\bullet(\gamma)$ with modest overhead compared to computing $\mathcal{D}_\bullet(X)$, and handles tens of thousands of points in \mathbb{R}^3 within seconds.

1. INTRODUCTION

Background and motivation. The *offset filtration* of a finite set $X \subset \mathbb{R}^d$ is a multi-scale representation of X which plays a major role in topological data analysis (TDA). By definition, this is the nested family of spaces $\mathcal{O}_\bullet(X) = (\mathcal{O}_r(X))_{r \geq 0}$, where $\mathcal{O}_r(X)$ is the union of closed balls of radius r centered at the points in X . The *persistent homology* of $\mathcal{O}_\bullet(X)$ is one of the most commonly computed objects in TDA. However, $\mathcal{O}_\bullet(X)$ is not a combinatorial object, and is therefore difficult to compute directly. So one instead usually computes the *Delaunay filtration* $\mathcal{D}_\bullet(X) = (\mathcal{D}_r(X))_{r \geq 0}$ (also called the α -filtration), a filtration of the Delaunay triangulation $\mathcal{D}(X)$ of X ; see Figure 1. By a functorial variant of the classical nerve theorem [6], $\mathcal{D}_\bullet(X)$ is topologically equivalent to $\mathcal{O}_\bullet(X)$ and therefore has the same persistent homology; see Section 3 for a formal definition of topological equivalence. For TDA computations with low-dimensional data, $\mathcal{D}_\bullet(X)$ is preferable to alternative simplicial filtrations such as the Čech and (Vietoris)-Rips filtrations because, as discussed below, it is asymptotically smaller and much more scalable in practice.

The index at which a simplex σ first appears in $\mathcal{D}_\bullet(X)$ is defined to be the minimum radius of an empty circumsphere of σ . If we instead define this index to be the radius of the minimum enclosing ball (meb) of σ , we obtain a topologically equivalent filtration, the *Delaunay-Čech filtration* $\mathcal{DC}_\bullet(X)$ [5].

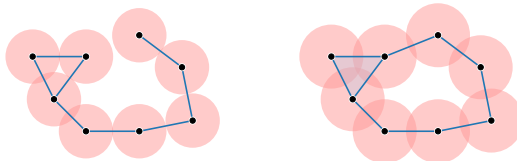


FIGURE 1. Offsets $\mathcal{O}_r(X) \subset \mathcal{O}_{r'}(X)$ (pink) and Delaunay complexes $\mathcal{D}_r(X) \subset \mathcal{D}_{r'}(X)$ (blue) of a point set $X \subset \mathbb{R}^2$.

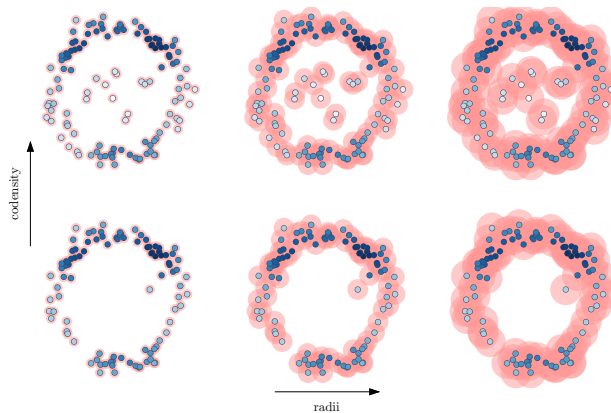


FIGURE 2. Part of the sublevel offset bifiltration $\mathcal{O}_\bullet(\gamma)$ of a codensity function $\gamma: X \rightarrow \mathbb{R}$, where $X \subset \mathbb{R}^2$. Lightness of shading is proportional to the value of γ .

The point set X often comes equipped with a function $\gamma: X \rightarrow \mathbb{R}$. One then wishes to refine the topological analysis of X to take γ into account. In some cases, γ is provided by an application; for example, if X is the set of atom centers of a biomolecule, γ may be a partial charge function [25, 26, 51]. In other cases, γ is constructed from X itself, e.g., as an estimate of curvature or codensity (e.g., the inverse or negation of a density function). The case where γ is a codensity estimate is particularly important in TDA because in the presence of outliers, $\mathcal{O}_\bullet(X)$ can be insensitive to topological structure in the high-density regions of X [28, 27].

Carlsson and Zomorodian [28] propose to analyze γ using *multiparameter persistence*, and specifically, to consider the *sublevel offset bifiltration* $\mathcal{O}_\bullet(\gamma) = (\mathcal{O}_{r,s}(\gamma))_{(r,s) \in A}$, where $A = [0, \infty) \times \mathbb{R}$, $\mathcal{O}_{r,s}(\gamma) = \mathcal{O}_r(X^s)$, and $X^s = \gamma^{-1}(-\infty, s]$ is the s -sublevel set of γ . This is indeed a bifiltration, in the sense that $\mathcal{O}_{r,s}(\gamma) \subset \mathcal{O}_{r',s'}(\gamma)$ whenever $r \leq r'$ and $s \leq s'$. Figure 2 illustrates the sublevel offset bifiltration of a codensity function.

As detailed below, multiparameter persistence is an active area of TDA, providing well-developed computational tools for working with bifiltrations and their persistent homology [20]. One would like to apply these tools to $\mathcal{O}_\bullet(\gamma)$, but as with $\mathcal{O}_\bullet(X)$, direct computation of $\mathcal{O}_\bullet(\gamma)$ is difficult. Thus, one wants an equivalent simplicial bifiltration that can be computed efficiently. The goal of this paper is to introduce such a bifiltration.

Contributions. In this work, we introduce the *sublevel Delaunay-Čech bifiltration* $\mathcal{DC}_\bullet(\gamma) = (\mathcal{DC}_{r,s}(\gamma))_{(r,s) \in A}$, a bifiltered analogue of $\mathcal{DC}_\bullet(X)$ which is topologically equivalent to $\mathcal{O}_\bullet(\gamma)$, provably small in size, and readily computed in practice. The definition of $\mathcal{DC}_\bullet(\gamma)$ is not obvious: one might hope to define $\mathcal{DC}_\bullet(\gamma)$ as a bifiltration of the Delaunay triangulation of X , but this fails because Delaunay triangulations are not monotonic with respect to insertion of new points; see Figure 3. We instead define $\mathcal{DC}_\bullet(\gamma)$ as a bifiltration of a novel simplicial complex $\mathcal{I}(\gamma)$ with vertex set X , the *incremental Delaunay complex*; see Definition 2.1. $\mathcal{I}(\gamma)$ contains the Delaunay triangulation of every sublevel set of γ , as well as additional simplices needed to encode the topological relationships between consecutive levels. $\mathcal{I}(\gamma)$ embeds in \mathbb{R}^{d+1} via the celebrated parabolic lift paradigm for Delaunay triangulations.

We characterize $\mathcal{I}(\gamma)$ in terms of two standard (and closely related) incremental constructions of Delaunay triangulations: the flipping algorithm [42, 57] and Bowyer-Watson algorithm [23, 72]. These characterizations make clear that both algorithms implicitly compute

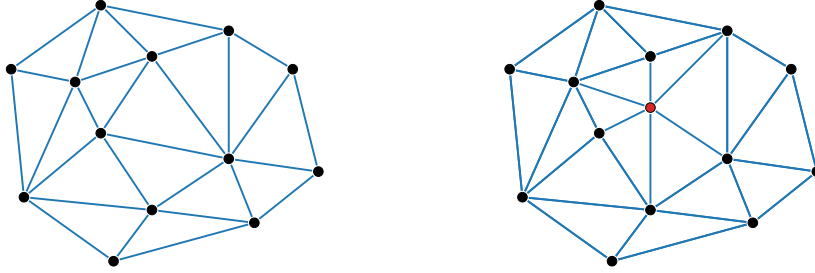


FIGURE 3. The Delaunay triangulations $\mathcal{D}(X)$ and $\mathcal{D}(Y)$ of planar point sets X (left) and $Y = X \cup \{y\}$ (right, with y in red). Note that $\mathcal{D}(X) \not\subset \mathcal{D}(Y)$.

$\mathcal{I}(\gamma)$. In fact, an implementation of either algorithm can be used off the shelf to explicitly compute $\mathcal{I}(\gamma)$ with just a few additional lines of code. Our code¹ computes $\mathcal{I}(\gamma)$ using CGAL’s implementation of the Bowyer-Watson algorithm in arbitrary dimensions [35] and GUDHI’s simplex tree data structure for simplicial complexes [17, 62].

Leveraging the characterization of $\mathcal{I}(\gamma)$ in terms of flips, we observe that $\mathcal{I}(\gamma)$ is of size $O(|X|^{\lceil \frac{d+1}{2} \rceil})$, assuming X in general position. The Delaunay triangulation $\mathcal{D}(X)$ has size $\Theta(|X|^{\lceil \frac{d}{2} \rceil})$ in the worst case, so for d odd, the worst-case sizes of $\mathcal{D}(X)$ and $\mathcal{I}(\gamma)$ are asymptotically equal. We use our size bound for $\mathcal{I}(\gamma)$ to show that computation of $\mathcal{I}(\gamma)$ requires time $O(|X|^{\lceil \frac{d}{2} \rceil + 1})$.

Given $\mathcal{I}(\gamma)$, we define $\mathcal{DC}_\bullet(\gamma)$ by taking $\sigma \in \mathcal{I}(\gamma)$ to appear in $\mathcal{DC}_\bullet(\gamma)$ at index $(r_\sigma, s_\sigma) \in A$, where r_σ is the radius of the meb of σ and $s_\sigma = \max_{x \in \sigma} \gamma(x)$. Alternatively, we can take each $\sigma \in \mathcal{I}(\gamma)$ to appear at index (ρ_σ, s_σ) , where ρ_σ is the radius of a smallest sphere witnessing that $\sigma \in \mathcal{I}(\gamma)$; see Definition 2.1. We call the resulting bifiltration $\mathcal{D}_\bullet(\gamma)$ the *sublevel Delaunay bifiltration*; this is a bifiltered analogue of $\mathcal{D}_\bullet(X)$. Both choices of radii can be efficiently computed, but since the computation of meb radii is conceptually simpler and efficient software is readily available for this² [43, 47], our experiments focus on $\mathcal{DC}_\bullet(\gamma)$. We prove that $\mathcal{D}_\bullet(\gamma)$, $\mathcal{DC}_\bullet(\gamma)$ and $\mathcal{O}_\bullet(\gamma)$ are topologically equivalent using Bauer and Edelsbrunner’s *selective Delaunay complexes* [5] and discrete Morse theory.

Our computational experiments demonstrate that our algorithm for computing $\mathcal{DC}_\bullet(\gamma)$ is highly effective in practice and, for low-dimensional Euclidean data, is far more scalable than the *sublevel Rips bifiltration*, a standard alternative construction discussed below. For instance, for 32000 points in \mathbb{R}^3 , $\mathcal{DC}_\bullet(\gamma)$ is computed in at most half a minute. This enables the application of 2-parameter persistence to much larger low-dimensional data sets than previously possible.

Related work. Besides $\mathcal{D}_\bullet(X)$, two other simplicial filtrations are commonly constructed from a point cloud $X \subset \mathbb{R}^d$, the *Čech* and *Rips filtrations* $\mathcal{C}_\bullet(X)$ and $\mathcal{R}_\bullet(X)$. Unlike $\mathcal{D}_\bullet(X)$, both the Čech and Rips filtrations extend straightforwardly to *sublevel Čech* and *sublevel Rips bifiltrations* $\mathcal{C}_\bullet(\gamma)$, $\mathcal{R}_\bullet(\gamma)$ of a function $\gamma: X \rightarrow \mathbb{R}$, in essentially the same way that $\mathcal{O}_\bullet(X)$ extends to $\mathcal{O}_\bullet(\gamma)$ [28]. Like $\mathcal{D}_\bullet(X)$, $\mathcal{C}_\bullet(X)$ is topologically equivalent to $\mathcal{O}_\bullet(X)$, and by Jung’s theorem [50], $\mathcal{R}_\bullet(X)$ is a 2-approximation to $\mathcal{O}_\bullet(X)$ (in the log-homotopy interleaving distance, see [13]); both results extend to the corresponding bifiltrations. $\mathcal{R}_\bullet(X)$ and $\mathcal{R}_\bullet(\gamma)$

¹https://bitbucket.org/mkerber/function_delaunay

²<https://people.inf.ethz.ch/gaertner/subdir/software/miniball.html>

have the advantage that their definition and computation extend naturally to arbitrary finite metric spaces.

The k -skeleta of both $\mathcal{R}_\bullet(X)$ and $\mathcal{C}_\bullet(X)$ have size $\Theta(|X|^{k+1})$, and the same is true for $\mathcal{C}_\bullet(\gamma)$ and $\mathcal{R}_\bullet(\gamma)$. Therefore, one computes the k -skeleta of these objects only for very small k (say, $k \leq 3$), which is sufficient for homology computations in dimension up to $k - 1$. Even so, the size of these (bi)filtrations can impede practical use. Therefore, for small values of d , it is usually preferable to work with $\mathcal{D}_\bullet(X)$ rather than $\mathcal{R}_\bullet(X)$ or $\mathcal{C}_\bullet(X)$.

That said, highly optimized methods have been developed for computing persistent homology of the (1-parameter) Rips filtrations of arbitrary finite metric spaces [4, 48, 18], and these are used widely. Recent work has focused on adapting some such optimizations to the computation of sublevel Rips bifiltrations [7, 2]. Sublevel Rips bifiltrations have recently been applied to problems in computational chemistry [51] and cancer imaging [71, 8]. As these applications involve low-dimensional Euclidean data, future applications along similar lines may benefit from instead using the Delaunay bifiltrations introduced in this paper. The standard approach to computing $\mathcal{C}_\bullet(X)$ [67] adapts to the computation of $\mathcal{C}_\bullet(\gamma)$, though to our knowledge this has not yet been implemented.

The problem of non-monotonicity of Delaunay triangulations has been considered in prior work by Reani and Bobrowski [65]. Given two point sets $X, Y \subset \mathbb{R}^d$, they introduce a computable *coupled Delaunay filtration* $\mathcal{A}_\bullet(X, Y)$ containing both $\mathcal{D}_\bullet(X)$ and $\mathcal{D}_\bullet(Y)$ as subfiltrations such that the zigzag

$$\mathcal{D}_\bullet(X) \hookrightarrow \mathcal{A}_\bullet(X, Y) \hookleftarrow \mathcal{D}_\bullet(Y)$$

is topologically equivalent to

$$\mathcal{O}_\bullet(X) \hookrightarrow \mathcal{O}_\bullet(X \cup Y) \hookleftarrow \mathcal{O}_\bullet(Y).$$

See also [38, 9] for a recent extension to three or more point sets. In the special case that $Y = X \cup \{p\}$, our main construction yields a filtration much smaller than $\mathcal{A}_\bullet(X, Y)$ with the same property. More generally, a construction similar to ours yields a smaller filtration whenever $X \cap Y \neq \emptyset$; we leave further discussion of this (including computational considerations) to future work.

When γ is a codensity function, the sublevel bifiltrations of γ enable data analysis that is sensitive to both density and spatial scale. However, one disadvantage of working with these bifiltrations is that such γ always depends on a choice of *bandwidth parameter*, and it is often unclear how to select this. Several density-sensitive bifiltrations have been proposed that do not depend on a bandwidth parameter [59, 12, 69], but these are more computationally costly than either $\mathcal{R}_\bullet(\gamma)$ or $\mathcal{D}_\bullet(\gamma)$. Most closely related to our work is the *rhomboid bifiltration*, introduced in [40] and studied in [32]. This is a polyhedral extension of $\mathcal{D}(X)$ which satisfies a strong robustness property [12] and is computable in polynomial time [41]. However, the rhomboid bifiltration of $X \subset \mathbb{R}^d$ has exactly $\binom{|X|}{d+1}$ top-dimensional cells, which means it is usually too large to fully compute.

In the computational pipeline of multiparameter persistence, our task of obtaining a bifiltration from a data set is just the first step; one then usually aims to compute and visualize *topological invariants* of the bifiltration [59, 28, 24, 68, 37]. Among the many invariants that have been proposed, *signed barcodes* are among the most actively studied [21, 55, 22, 63, 3, 11, 64]. There is also substantial interest in invariants taking values in linear spaces, since these are readily incorporated into standard machine learning and statistics pipelines [61, 70, 31, 29, 74]. One can also work with 2-parameter persistent homology

via *distance functions* [53, 1, 10, 51]. All of these approaches are computationally challenging and are most practical when the input bifiltration is small; this is the practical motivation of our work. As an intermediate step in the computation of invariants, it is often beneficial to employ algebraic compression techniques to replace the bifiltration with a smaller object, for instance by computing a minimal representation of homology. Such compressed representations can often be computed with surprising efficiency in the 2-parameter setting [46, 60, 2, 7]. Our approach can be easily combined with these techniques, as we show in our experimental evaluation.

Outline. In Section 2, we define the incremental Delaunay complex, discuss its computation, and bound its size. In Section 3, we formally define topological equivalence and state the main topological equivalence results of this work, which are proven in Appendix A. In Section 4, we report on our experimental evaluations. We conclude in Section 5.

2. THE INCREMENTAL DELAUNAY COMPLEX

A circumsphere of $Q \subset \mathbb{R}^d$ is a $(d - 1)$ -sphere S such that all points in Q lie on S . Throughout the paper, we assume that our point sets are in general position, meaning that every non-empty subset $Q \subset X$ of at most $d + 1$ points is affinely independent, and no point of $X \setminus Q$ lies on the smallest circumsphere of Q . The *Delaunay triangulation* of X is the simplicial complex $\mathcal{D}(X)$ whose simplices are non-empty subsets $\sigma \subset X$ having an empty circumsphere S , that is, no points of X lies inside S .

Given a function $\gamma: X \rightarrow \mathbb{R}$, we totally order X by values of γ , breaking any ties arbitrarily. We write $X = \{x_1, x_2, \dots, x_{|X|}\}$ and for $i \in \{1, \dots, |X|\}$, we let $X_i \subset X$ denote the first i points of X . For a simplex $\sigma \subset X$, let $\max(\sigma)$ be the maximum point in σ .

Our definition of the incremental Delaunay complex $\mathcal{I}(\gamma)$ will depend only on the order on X , and not on the specific values taken by γ . Hence, we write $\mathcal{I}(X) = \mathcal{I}(\gamma)$.

Definition 2.1. The *incremental Delaunay complex* $\mathcal{I}(X)$ is the simplicial complex whose simplices are the non-empty subsets $\sigma \subset X$ such that there exists a circumsphere S of $\sigma \setminus \max(\sigma)$ satisfying the following two properties:

- $\max(\sigma)$ is either inside or on S and,
- each $x_i < \max(\sigma)$ is either outside or on S .

We call the infimal radius of such S the *incremental Delaunay radius* of σ , and denote it as ρ_σ .

Thus, writing $x_k := \max(\sigma)$, the sphere S of Definition 2.1 must be empty of points in X_{k-1} and x_k must be either on or inside S . There exists such S with x_k on S if and only if $\sigma \in \mathcal{D}(X_k)$. It follows that $\bigcup_{i=1}^{|X|} \mathcal{D}(X_i) \subset \mathcal{I}(X)$. Note also that $\mathcal{I}(X_i) \subset \mathcal{I}(X_j)$ whenever $i \leq j$, i.e., the incremental Delaunay complex is monotone under point insertions.

Computation. We now explain how $\mathcal{I}(X)$ can be computed via the Bowyer-Watson algorithm. Besides containing $\mathcal{D}(X_i)$ for each i , $\mathcal{I}(X)$ usually contains additional simplices of dimension $d + 1$ and their faces. To elaborate, for a d -simplex $\sigma \in \mathcal{D}(X_i)$, we will say that the pair (σ, x_{i+1}) is a *conflict pair* if x_{i+1} is inside the circumsphere of σ . We also call σ an *i -conflict*, or simply a *conflict*. By definition, we then have $\sigma \cup \{x_{i+1}\} \in \mathcal{I}(X)$, and all $(d + 1)$ -simplices of $\mathcal{I}(X)$ arise from conflict pairs in this way. We summarize this finding:

Lemma 2.2. *The $(d + 1)$ -simplices in $\mathcal{I}(X)$ are in one-to-one-correspondence with conflict pairs.*

We would like to leverage Lemma 2.2 to compute $\mathcal{I}(X)$, by computing all conflict pairs. But in general, the $(d + 1)$ -simplices of $\mathcal{I}(X)$ and their faces do not yield the entire complex $\mathcal{I}(X)$. The reason is that a point x_{i+1} might lie outside the convex hull of X_i , without giving rise to any conflict pair. Such cases can be avoided if we assume that the simplex spanned by the first $d + 1$ points of X is the convex hull of X ; we call this the Δ -property. As we explain in Remark 2.4 below, for the purpose of computing $\mathcal{I}(X)$, this assumption entails no loss of generality.

Assuming the Δ -property, any x_{i+1} with $i + 1 > d + 1$ lies in the convex hull of the previous points, and thus inside some d -simplex σ of $\mathcal{D}(X_i)$, which implies that (σ, x_{i+1}) is a conflict pair. It is then plausible that the $(d + 1)$ -simplices of $\mathcal{I}(X)$ fully determine $\mathcal{I}(X)$. The next lemma asserts that this is indeed true:

Lemma 2.3. *If $|X| \geq d + 2$ and X has the Δ -property, then every simplex of $\mathcal{I}(X)$ is a face of a $(d + 1)$ -simplex.*

Proof. Consider the simplex $\alpha = [x_1, \dots, x_{d+1}]$. By the Δ -property and the fact that $|X| \geq d + 2$, the point x_{d+2} lies in α . Hence (α, x_{d+2}) is a conflict pair, so α is a face of the simplex $[x_1, \dots, x_{d+2}]$ in $\mathcal{I}(X)$. Now assume for a contradiction that a simplex $\tau \in \mathcal{I}(X)$ with $\dim(\tau) < d + 1$ is maximal (i.e., has no proper coface). Let $x_{i+1} = \max(\tau)$ and $\tau' = \tau \setminus \{x_{i+1}\}$. As α is not maximal, we have $i + 1 \geq d + 2$.

We claim that $\tau \in \mathcal{D}(X_{i+1})$. For all upcoming notation, see Figure 4 for illustrations. By the definition of $\mathcal{I}(X)$, there is a circumsphere S of τ' such that x_{i+1} is either on or inside S , and no point of X_i lies inside S . Let S' be a circumsphere of τ ; this exists by general position and the assumption that $\dim(\tau) < d + 1$. We will show that no point of X_i lies inside S' , which proves the claim. Since both S and S' are circumspheres of τ' , there exists a collection $(S_t)_{t \in [0,1]}$ of circumspheres of τ' interpolating between S and S' ; that is, $S_0 = S$, $S_1 = S'$, and the radius and center of S_t both vary continuously with t . We call this collection a *pencil*. In fact, we can choose the pencil so that x_{i+1} lies on or inside each S_t . Recall that no point of X_i lies inside S . Thus, if a point of X_i lies inside S' , continuity of the pencil implies that there is a circumsphere S'' in the pencil for which a point p of $X_i \setminus \tau$ lies on S'' and no point of X_i lies inside S'' . Then, since x_{i+1} lies on or inside S'' , $\tau \cup \{p\}$ is a simplex of $\mathcal{I}(X)$, and hence τ is not maximal, a contradiction. We conclude that no point of X_i lies inside S' , and hence that $\tau \in \mathcal{D}(X_{i+1})$, as claimed.

Since $\tau \in \mathcal{D}(X_{i+1})$ and all maximal simplices of $\mathcal{D}(X_{i+1})$ are of dimension d , we have $\dim(\tau) = d$. The sphere S' also witnesses that $\tau' \in \mathcal{D}(X_i)$. Since τ' is a $(d - 1)$ -simplex, there exist either two d -dimensional cofaces σ, σ' of τ in $\mathcal{D}(X_i)$, or (when τ' is a convex hull simplex) only one such coface σ . In the former case, since τ is coface of τ' in $\mathcal{D}(X_{i+1})$, one of the d -simplices, say σ , is not in $\mathcal{D}(X_{i+1})$. In the latter case, σ is not in $\mathcal{D}(X_{i+1})$ either, because otherwise τ' would not be on the convex hull anymore, contradicting the Δ -property. In either case, this implies that x_{i+1} lies inside the circumsphere of σ , and hence (σ, x_{i+1}) is a conflict pair. However, since τ' is a face of σ , the simplex $\sigma \cup \{x_{i+1}\}$ is a coface of τ , a contradiction. \square

Lemmas 2.2 and 2.3 imply that if X has the Δ -property, then to compute $\mathcal{I}(X)$ it suffices to determine all conflict pairs. These pairs are computed by the Bowyer-Watson algorithm [23, 72], a standard incremental algorithm for Delaunay triangulation computation, which we now

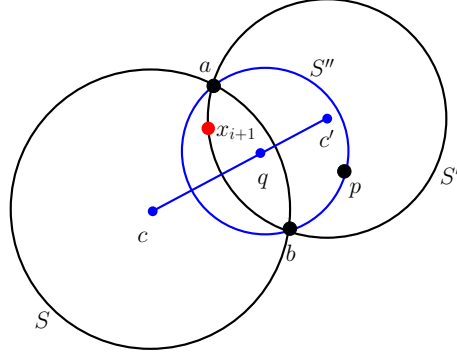


FIGURE 4. Illustration of the proof of Lemma 2.3. Here, $X_i = \{a, b, p\}$ and $\tau = \{a, b, x_{i+1}\}$. Note that S contains no point of X_i by assumption, whereas S' might contain such points (like p in the figure).

recall in outline; see also Figure 5. Given $\mathcal{D}(X_i)$, to compute $\mathcal{D}(X_{i+1})$ the algorithm computes all i -conflicts. These simplices are removed from the triangulation, leaving an untriangulated star-convex region R with center x_{i+1} . R is then retriangulated by the simplicial cone with base the boundary of R and apex x_{i+1} , yielding $\mathcal{D}(X_{i+1})$.

To compute all i -conflicts, we must first compute one of them; we call this step *conflict location*. Since R is connected, once we have found a single i -conflict, we can efficiently find the remaining ones by searching the adjacency graph of the d -simplices of $\mathcal{D}(X_i)$. A naive conflict location strategy (which nevertheless suffices for our complexity analysis below) is to iterate through the d -simplices of $\mathcal{D}(X_i)$ until a conflict is found. Alternatively, a standard approach is to maintain a data structure for efficient point location, which can then be queried for the d -simplex containing x_{i+1} . Several such data structures have been proposed and implemented [34, 36, 19, 15]. Our code uses CGAL's implementation of point location.

Remark 2.4. To ensure that the Δ -property holds, we can augment X with a set T of $(d+1)$ extra points ordered below X . Choosing the points of T to be sufficiently far away from X ensures that $\mathcal{I}(X)$ is the subcomplex of $\mathcal{I}(X \cup T)$ obtained by removing all points of T and their cofaces. This is a standard technique in geometric algorithms; see for instance [33, Sec 9.3]. T need not be chosen explicitly, but can be handled symbolically; in fact, it suffices to add a single *point at infinity*, as in [16].

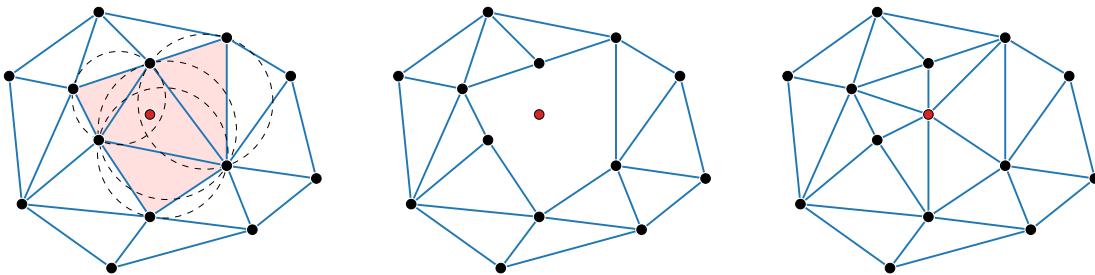


FIGURE 5. The Bowyer-Watson algorithm. Left: $\mathcal{D}(X_i)$ (blue) and x_{i+1} (red). The triangles in conflict with x_{i+1} are shaded. Center: These triangles are removed. Right: the hole is retriangulated, yielding $\mathcal{D}(X_{i+1})$.

Size of $\mathcal{I}(X)$. Assuming the Δ -property and that d is constant, Lemmas 2.2 and 2.3 together imply that $\mathcal{I}(X)$ has $O(m)$ simplices, where m is the total number of conflict pairs encountered by Bowyer-Watson algorithm. As we explain below,

Proposition 2.5. $m = O(|X|^{\lceil (d+1)/2 \rceil})$ in the worst case.

Proposition 2.5 implies the following, which in view of Remark 2.4, holds even when X does not satisfy the Δ -property:

Theorem 2.6. $\mathcal{I}(X)$ has $O(|X|^{\lceil (d+1)/2 \rceil})$ simplices.

The worst-case size of $\mathcal{D}(X)$ is $O(|X|^{\lceil d/2 \rceil})$, which for odd dimensions matches our size bound for $\mathcal{I}(X)$.

As we will explain, Proposition 2.5 follows from a result of Edelsbrunner and Shah [42] about *incremental flipping*, another well-known algorithm for computing Delaunay triangulations. Alternatively, we can easily deduce Proposition 2.5 by adapting the proof of [14, Theorem 3.10], a complexity bound for an incremental convex hull algorithm, but we will not discuss this approach.

Before proving Proposition 2.5, we recall the incremental flipping algorithm: Assuming the Δ -property for X again, the algorithm computes $\mathcal{D}(X_{i+1})$ from $\mathcal{D}(X_i)$ as follows (see Figure 6): The convex hull of $d+2$ points in general position has exactly two triangulations; the replacement of one with another is called a *flip*. We first subdivide the d -simplex of $\mathcal{D}(X_i)$ containing x_{i+1} into $d+1$ d -simplices, each with x_{i+1} as a vertex. We then transform the resulting triangulation into $\mathcal{D}(X_{i+1})$ via flips in the following way. Let T be the triangulation we maintain during the algorithm. For a d -simplex σ in T with vertex x_{i+1} , let $\hat{\sigma} = \sigma \setminus \{x_{i+1}\}$. There is at most one vertex $y_\sigma \neq x_{i+1}$ such that $\hat{\sigma} \cup \{y_\sigma\} \in T$. We say σ is *flippable* if y_σ is inside the circumsphere of σ . While there exists a flippable simplex σ in T , we update T by doing a flip on the restriction of T to $\sigma \cup \{x_{i+1}, y_\sigma\}$. When there are no more flippable simplices, we have $T = \mathcal{D}(X_{i+1})$ and the computation is complete.

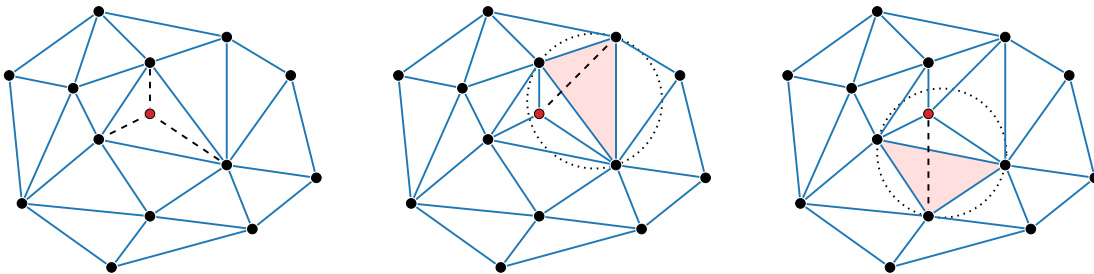


FIGURE 6. Incremental flipping. Left: we insert a new point x_{i+1} (red) into $\mathcal{D}(X_i)$ (blue); the dashed edges are the result of the initial subdivision step. Center: the highlighted triangle is in conflict with x_{i+1} and needs to be flipped; the dashed edge is inserted and the solid edge it crosses is removed. Right: we continue flipping the rest of triangles that are in conflict.

Proof of Proposition 2.5. It is easily checked that for each flippable simplex σ encountered by the incremental flipping algorithm, we have $\hat{\sigma} \cup \{y_\sigma\} \in \mathcal{D}(X_i)$ and therefore, $(\hat{\sigma} \cup \{y_\sigma\}, x_{i+1})$ is a conflict pair. Conversely, if a simplex (τ, x_{i+1}) is a conflict pair, then $\tau \cup \{x_{i+1}\}$ must be involved in a flip. Thus, as no flip is done more than once [42, Sec 8], the total number of flips done by the algorithm equals the total number of conflict pairs. The number of

flips is shown in [42, Sec 9] to be $O(|X|^{\lceil (d+1)/2 \rceil})$ in the worst case, by counting simplices in dimension $\lfloor \frac{d}{2} \rfloor$. \square

Cost of computing $\mathcal{I}(X)$. Computing $\mathcal{I}(X)$ via Bowyer-Watson requires time $O(|X|^{\lceil d/2 \rceil + 1})$. To explain, the cost is dominated by the cost of finding all conflicts. Once we have located an i -conflict, the cost of finding the remaining i -conflicts is linear in the number of i -conflicts. Thus, since $\mathcal{I}(X)$ has one $(d+1)$ -simplex for each conflict, the cost of finding all conflicts admits an output-sensitive bound of $O(m+n)$, where $m = O(|X|^{\lceil (d+1)/2 \rceil})$ is the size of $\mathcal{I}(X)$ and n is the total cost of locating an i -conflict for each i . Using the naive strategy of iterating through the simplices of $\mathcal{D}(X_i)$, locating an i -conflict requires time $O(n_i) = O(|X_i|^{\lceil d/2 \rceil})$, where n_i is the number of d -simplices in $\mathcal{D}(X_i)$. Hence $n = O(\sum_i n_i) = O(|X|^{\lceil d/2 \rceil + 1})$ and $m+n$ satisfies the same bound.

We are not aware of any conflict location strategy in the literature that achieves a better bound on n . The key difficulty is that to compute $\mathcal{I}(X)$, the order of point insertion must be compatible with γ . In contrast, we can compute $\mathcal{D}(X)$ by inserting points in arbitrary order. A standard analysis shows when the points are inserted in random order, Bowyer-Watson computes $\mathcal{D}(X)$ in expected time $O(|X|^{\lceil d/2 \rceil} + |X| \log |X|)$; the randomness lowers both the cost of point location and the number of conflicts, in expectation. But we cannot use a random insertion order to compute $\mathcal{I}(X)$.

The lifting perspective. Define $f: \mathbb{R}^d \rightarrow \mathbb{R}^{d+1}$ by $f(x) = (x, \|x\|^2)$. It is well known that $\mathcal{D}(X)$ is the image of the lower hull of $f(X)$ under the projection $\mathbb{R}^{d+1} \rightarrow \mathbb{R}^d$ that drops the last coordinate. Thus, this lower hull, which we call the *lift of $\mathcal{D}(X)$* , is an embedding of $\mathcal{D}(X)$ in \mathbb{R}^{d+1} .

This embedding extends to an embedding of $\mathcal{I}(X)$ whose lower envelope is the lift of $\mathcal{D}(X)$; see Figure 7. It is helpful to think about this embedding in terms of the lifts of consecutive pairs of Delaunay triangulations $\mathcal{D}(X_i)$, $\mathcal{D}(X_{i+1})$. If x_{i+1} lies in the convex hull of X_i , then the lift of $\mathcal{D}(X_{i+1})$ partially coincides with the lift of $\mathcal{D}(X_i)$ and otherwise lies below it in the x_{d+1} -direction. The two lifts enclose a void in \mathbb{R}^{d+1} . The upper hull of this void consists of all d -simplices in $\mathcal{D}(X_i)$ that do not belong to $\mathcal{D}(X_{i+1})$; the lower hull consists of the d -simplices in $\mathcal{D}(X_{i+1})$ containing x_{i+1} . Noting that $f(x_{i+1})$ lies below the hyperplane of each d -simplex in the upper hull of the void, one can check that the $(d+1)$ -simplices of $\mathcal{I}(X_{i+1}) \setminus \mathcal{I}(X_i)$ triangulate the void.

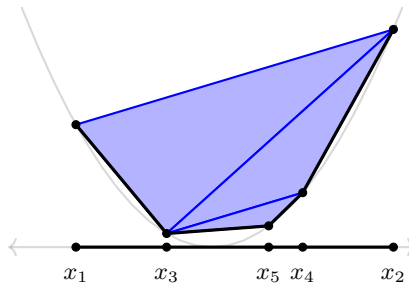


FIGURE 7. The Delaunay triangulation $\mathcal{D}(X)$ of a set of five points $X \subset \mathbb{R}$ and its parabolic lift are drawn in black. $\mathcal{I}(X)$ is drawn in blue for the order of X shown.

3. SUBLEVEL BIFILTRATIONS

Simplicial bifiltrations of point clouds. As in the introduction, let $A = [0, \infty) \times \mathbb{R}$, and define the sublevel Delaunay-Čech and sublevel Delaunay bifiltrations of $\gamma: X \rightarrow \mathbb{R}$, denoted $\mathcal{DC}_\bullet(\gamma)$ and $\mathcal{D}_\bullet(\gamma)$, to be the A -indexed bifiltrations given by

$$\begin{aligned}\mathcal{DC}_{r,s}(\gamma) &= \{\sigma \in \mathcal{I}(X) \mid r_\sigma \leq r, \gamma(\max(\sigma)) \leq s\}, \\ \mathcal{D}_{r,s}(\gamma) &= \{\sigma \in \mathcal{I}(X) \mid \rho_\sigma \leq r, \gamma(\max(\sigma)) \leq s\}.\end{aligned}$$

where r_σ denotes the radius of the minimum enclosing ball of σ and ρ_σ is the incremental Delaunay radius of Definition 2.1.

To establish the topological equivalence of these bifiltrations and the sublevel offset bifiltration $\mathcal{O}_\bullet(\gamma)$ defined in the introduction, we also consider the sublevel Čech bifiltration $\mathcal{C}_\bullet(\gamma)$. Recall that Čech filtration $\mathcal{C}_\bullet(X)$ is the $[0, \infty)$ -indexed filtration defined by

$$\mathcal{C}_r(X) = \{\sigma \subset X \mid \bigcap_{x \in \sigma} B_r(x) \neq \emptyset\},$$

where $B_r(x)$ denotes the closed ball of radius r centered at x . We then define $\mathcal{C}_\bullet(\gamma)$ to be the A -indexed bifiltration given by $\mathcal{C}_{r,s}(\gamma) = \mathcal{C}_r(\gamma^{-1}(-\infty, s])$. In analogy to the 1-parameter setting [5], these bifiltrations are related by containment as follows:

$$\mathcal{D}_\bullet(\gamma) \subset \mathcal{DC}_\bullet(\gamma) \subset \mathcal{C}_\bullet(\gamma).$$

Topological equivalence of bifiltrations. We next consider a notion of topological equivalence of (bi)filtrations which is standard in classical algebraic topology and also naturally suited to TDA [32, 13, 6, 56]. We will write the definition only for A -indexed bifiltrations, but the definitions extend to 1-parameter filtrations and more generally, to diagrams of topological spaces indexed by an arbitrary partially ordered set. Given A -indexed bifiltrations of topological spaces F_\bullet and G_\bullet , a *natural transformation* $\alpha: F_\bullet \rightarrow G_\bullet$ is a collection of continuous maps $(\alpha_a: F_a \rightarrow G_a)_{a \in A}$ such that the following diagram commutes for every $a \leq a'$:

$$\begin{array}{ccc} F_a & \hookrightarrow & F_{a'} \\ \alpha_a \downarrow & & \downarrow \alpha_{a'} \\ G_a & \hookrightarrow & G_{a'} \end{array}$$

We say that α is a *pointwise homotopy equivalence* if each α_a is a homotopy equivalence. Existence of a pointwise homotopy equivalence $F_\bullet \rightarrow G_\bullet$ is not an equivalence relation on bifiltrations, but it generates one:

Definition 3.1. F_\bullet and G_\bullet are said to be *topologically equivalent* (or *weakly equivalent*) if they are connected by a zigzag of pointwise homotopy equivalences:

$$\begin{array}{ccccccc} & & \mathcal{C}_\bullet^1 & & \dots & & \mathcal{C}_\bullet^m \\ & \swarrow & & \searrow & & \swarrow & \searrow \\ F_\bullet & & & & & & G_\bullet \\ & \searrow & & \swarrow & & \searrow & \\ & & \mathcal{C}_\bullet^2 & & \mathcal{C}_\bullet^{m-1} & & \end{array}$$

The following is an immediate consequence of the (functorial) Nerve Theorem [6, Thm 3.9]:

Proposition 3.2. $\mathcal{C}_\bullet(\gamma)$ and $\mathcal{O}_\bullet(\gamma)$ are topologically equivalent.

To compare the topology of $\mathcal{DC}_\bullet(\gamma)$, $\mathcal{D}_\bullet(\gamma)$, and $\mathcal{C}_\bullet(\gamma)$, we work with *collapses*, a combinatorial notion of deformation retraction first introduced by Whitehead [73, 39]. In a simplicial complex K , a simplex σ is a *free face* of a simplex τ if τ is the only simplex that properly contains σ . There is an *elementary collapse* from K to a subcomplex L if $K \setminus L$ is a pair of simplices $\{\sigma, \tau\}$ such that σ is a free face of τ . We say that K *collapses* to L and write $K \searrow L$ if there is a sequence of elementary collapses from K to L . If $K \searrow L$, then the inclusion $L \hookrightarrow K$ is a homotopy equivalence.

In Appendix A, we prove the following theorem:

Theorem 3.3. *For any $a \in [0, \infty) \times \mathbb{R}$,*

$$\mathcal{C}_a(\gamma) \searrow \mathcal{D}_a(\gamma) \text{ and } \mathcal{DC}_a(\gamma) \searrow \mathcal{D}_a(\gamma).$$

As an immediate corollary, we obtain the main topological result of this paper:

Corollary 3.4. *The inclusions of filtrations*

$$\mathcal{D}_\bullet(\gamma) \hookrightarrow \mathcal{DC}_\bullet(\gamma) \text{ and } \mathcal{D}_\bullet(\gamma) \hookrightarrow \mathcal{C}_\bullet(\gamma)$$

are both pointwise homotopy equivalences. Hence $\mathcal{D}_\bullet(\gamma)$, $\mathcal{DC}_\bullet(\gamma)$, $\mathcal{C}_\bullet(\gamma)$, and $\mathcal{O}_\bullet(\gamma)$ are all topologically equivalent.

4. IMPLEMENTATION AND EXPERIMENTS

We have written a C++ program to compute the sublevel Delaunay-Čech bifiltration $\mathcal{DC}_\bullet(\gamma)$ of a function $\gamma: X \rightarrow \mathbb{R}$, where $X \subset \mathbb{R}^d$ and $d \geq 2$. It reads a text file containing $(d+1)$ float values per line; each line specifies a point in $x \in X$, with $\gamma(x)$ as the last value. The program computes a graded chain complex representing $\mathcal{DC}_\bullet(\gamma)$ in the SCC2020 file format [52]. When $d = 2$ or $d = 3$, the program uses CGAL’s specialized Delaunay triangulations for these dimensions [75, 49]; when $d > 3$, it uses CGAL’s implementation of Delaunay triangulations for arbitrary dimensions [35].

After augmenting X to enforce the Δ -property as in Remark 2.4, our program computes all $(d+1)$ -simplices of the incremental Delaunay complex using the variant of the Bowyer-Watson algorithm described in Section 2. These simplices are inserted into a *simplex tree* [17], an efficient data structure for simplicial complexes available in GUDHI [62]. The meb radii of all simplices are then computed using CGAL [43] (for $d \leq 10$) or the software package MINIBALL by Gärtner³ (for $d > 10$). For efficiency, we compute the meb radii in order of decreasing simplex dimension, exploiting the fact that if the meb of σ contains $\tau \subset \sigma$ in its interior, then the same ball is also the meb of $\sigma \setminus \tau$. Finally, the simplices are ordered with respect to their meb radius, the function value of each simplex is determined, and the output file is written.

Thanks to its use of the aforementioned software packages, our program consists of only around 1500 lines of code. We offer it in a public repository⁴ published under the GNU Public License (GPL).

All experiments were performed on a computer with an Intel Core i7-5960X CPU @ 3.00GHz and 64GB of memory, running Ubuntu 20.04.6 LTS. The program was compiled with g++ 9.4.0.

³<https://people.inf.ethz.ch/gaertner/subdir/software/miniball.html>

⁴https://bitbucket.org/mkerber/function_delaunay

Datasets. We have generated various point clouds by sampling 1-spheres S^1 and unit squares $[0, 1]^2$ in \mathbb{R}^2 , and 2-spheres S^2 , tori $S^1 \times S^1$ and unit cubes $[0, 1]^3$ in \mathbb{R}^3 . For each point cloud, we add 5% of noise, sampled from the uniform distribution. In addition, a small perturbation (5%) is introduced to each point cloud to ensure that point clouds are in general position. For each of these five data types, we considered samples of 500, 1000, 2000, 4000, 8000, 16000 and 32000 points. For fixed type and number of points, we generated five independent samples, resulting in 125 different point clouds.

For each point cloud, we tested the following four choices of functions

- *codensity function* $\gamma(p) = - \sum_{q \neq p} \exp\left(-\frac{\|p-q\|^2}{\sigma^2}\right)$, with σ chosen as 0.1st percentile of the non-zero distances between points in X .
- *L_1 -coeccentricity* $\text{ecc}_1(p) = - \sum_{q \in X} \frac{\|p-q\|}{|X|}$, where $|X|$ denotes the size of X .
- *height* $h(p) = p_d$, where p_d is the last coordinate of $p \in \mathbb{R}^d$
- *random*, where each points gets an independent, random value in $[0, 1]$.

In total, our test suite contains a total of 500 point clouds with functions. For brevity, in what follows we only present a subset of representative results.

Complex size. To get a sense of how large incremental Delaunay triangulations are in practice, we experimentally compare the sizes of incremental Delaunay complexes and Delaunay triangulations. Table 1 gives such a comparison for points on the circle in \mathbb{R}^2 and on the torus in \mathbb{R}^3 . There are two major observations: first, for randomly assigned function values, the ratio of the sizes remains (nearly) constant. That is expected, as this case corresponds to the randomized incremental construction (RIC) paradigm, and it is known that the size of the RIC is small in expectation. The second observation is that the non-random functions lead to bigger incremental Delaunay complex, and moreover, the ratio of the sizes is growing as the number of points grows. While we cannot offer a theoretical explanation of this behavior, we suspect that the insertion order of the points is particularly disadvantageous for the incremental construction: for instance, in the height function, every newly inserted point is outside of the convex hull of the previous points which is not typical for RIC. Nevertheless, we observe that the ratio grows slowly and is rather small, making the computation of the incremental Delaunay complex still feasible for large point clouds in small dimension.

Computation time. We report on the time and memory to compute the sublevel Delaunay bifiltration (in chain complex format) in Table 2. Time for file IO is not reported. We observe a slightly super-linear performance for all function choices. That is expected from the previous experiments for the non-random functions since the size of the output complex grows super-linear as well, but remarkably, also applies to random function values, although the growth seems slightly smaller. We also normalized the runtime by dividing it by the complex size, and we observe that the time spent per simplex tends to grow for larger instances. Nevertheless, despite an apparent super-linear behavior with respect to the output size, the program can compute bifiltrations for tens of thousands of points in \mathbb{R}^3 within less than a minute. Also, the memory consumption is close to linear.

Comparison with sublevel Rips. We next compare the performance of homology computations using sublevel Delaunay-Čech and sublevel Rips bifiltrations. Still fixing a point set X and a function $\gamma : X \rightarrow \mathbb{R}$, the sublevel Rips bifiltration $\mathcal{R}_\bullet(\gamma)$ is defined by taking $\mathcal{R}_{r,s}(\gamma)$ to consist of all cliques $S \subset X$ of diameter at most r whose points have γ -value

Sample	#Points	Delaunay size	Random		Density		Height		Eccentricity	
			Size	Ratio	Size	Ratio	Size	Ratio	Size	Ratio
S^1	1000	5975	19481	3.26	23611	3.95	25575	4.28	39419	6.6
	2000	11971	39131	3.27	49593	4.14	57019	4.76	83209	6.95
	4000	23959	79839	3.33	102307	4.27	127111	5.31	180307	7.53
	8000	47967	158789	3.31	209099	4.36	282055	5.88	375891	7.84
	16000	95953	318919	3.32	430991	4.49	619561	6.46	788465	8.22
	32000	191943	638553	3.33	889599	4.63	1343567	7.0	1638579	8.54
$S^1 \times S^1$	1000	27003	122181	4.52	171105	6.34	230075	8.52	215815	7.99
	2000	52717	257129	4.88	361151	6.85	515437	9.78	467803	8.87
	4000	105249	512521	4.87	747617	7.1	1159641	11.02	937369	8.91
	8000	211885	1010347	4.77	1526509	7.2	2561545	12.09	1911169	9.02
	16000	426531	2028761	4.76	3093869	7.25	5578187	13.08	3912707	9.17
	32000	862789	4065635	4.71	6376129	7.39	12145149	14.08	8118607	9.41

TABLE 1. Size comparison of incremental Delaunay complexes and Delaunay triangulations.

Sample	#Points	Random			Density			Height			Eccentricity		
		Time (s)	Time/simplex (ms)	Memory (GB)	Time (s)	Time/simplex (ms)	Memory (MB)	Time (s)	Time/simplex (ms)	Memory (MB)	Time (s)	Time/simplex (ms)	Memory (MB)
S^1	1000	0.03	1.58	8.44	0.05	2.01	9.4	0.04	1.5	9.72	0.05	1.35	13.12
	2000	0.06	1.62	12.87	0.08	1.54	15.08	0.08	1.33	17.14	0.14	1.67	22.79
	4000	0.13	1.69	21.88	0.16	1.58	26.48	0.17	1.36	32.86	0.3	1.66	44.19
	8000	0.28	1.78	39.56	0.35	1.68	50.13	0.44	1.55	68.38	0.64	1.71	87.75
	16000	0.64	2.02	74.72	0.81	1.87	98.46	1.03	1.66	146.57	1.44	1.82	178.85
	32000	1.5	2.35	147.81	1.79	2.01	199.02	2.37	1.76	311.03	3.17	1.94	371.64
$S^1 \times S^1$	1000	0.21	1.73	31.89	0.3	1.77	43.03	0.41	1.79	57.21	0.38	1.76	53.09
	2000	0.49	1.92	62.76	0.75	2.06	85.69	1.05	2.03	125.26	0.95	2.04	110.82
	4000	1.11	2.17	122.72	1.59	2.12	170.57	2.44	2.1	265.98	1.98	2.11	224.83
	8000	2.36	2.34	236.03	3.49	2.29	354.77	5.54	2.16	619.1	4.17	2.18	437.08
	16000	5.11	2.52	455.98	7.41	2.4	710.66	12.7	2.28	1271.56	8.94	2.28	910.05
	32000	11.1	2.73	929.58	15.65	2.45	1461.12	28.5	2.35	2796.81	19.08	2.35	1847.01

TABLE 2. Running time (in seconds), the average time to process a simplex (in millisecond), and the memory consumption (in MB) for computing the sublevel Delaunay bifiltration.

at most s . As noted in the introduction, because the full sublevel Rips bifiltration $\mathcal{R}_\bullet(\gamma)$ is large, we usually consider its k -skeleton for k small. Here we will take $k = 2$, which is sufficient for homology computations of degree at most one. Still, the 2-skeleton of $\mathcal{R}_\bullet(\gamma)$ has a cubic number of simplices in $|X|$, which is prohibitively large for the data sizes we consider.

However, recent work has introduced way to compute a smaller but equivalent bifiltration: Note that for r and s large enough, $\mathcal{R}_{r,s}(\gamma)$ is a clique complex over a complete graph. Alonso, Kerber, and Pritam [2] preprocess the complete graph by removing edges to arrive at a smaller graph G , and show that the bifiltration $\mathcal{G}_\bullet(\gamma)$ induced by the clique complex of G is equivalent to $\mathcal{R}_\bullet(\gamma)$.

Given a simplicial filtration \mathcal{Z} , the software *mpfree*⁵ [60, 54, 46] efficiently computes a minimal presentation of the homology of \mathcal{Z} in a fixed degree.

We use *mpfree* and the code from [2]⁶ to compute (a minimal presentation of) the homology of $\mathcal{R}_\bullet(\gamma)$ in degree 1. We also use *mpfree* to compute the homology of $\mathcal{I}(\gamma)$ in degree 1.

⁵<https://bitbucket.org/mkerber/mpfree/src/master/>

⁶https://github.com/aj-alonso/filtration_domination

These computations require us only to compute the 2-skeleta of $\mathcal{G}_\bullet(\gamma)$ and $\mathcal{I}_\bullet(\gamma)$. We note that the results of the two computations are *not* equivalent, because $\mathcal{R}_\bullet(\gamma)$ is not topologically equivalent to $\mathcal{O}_\bullet(\gamma)$. However, as indicated in the introduction, the two bifiltrations approximate each other, and hence the same is true for their homology [13].

Table 3 shows the results of our comparison. We see that our approach improves on the Rips variant in terms of complex size, time, and memory, usually by several orders of magnitude. This is the case even though the approach of [2] substantially reduces the number of edges in the bifiltration and therefore vastly improves on a naive computational strategy [2].

The software *2pac*⁷, based on recent work of Bauer, Lenzen, and Lesnick [7], is an alternative to *mpfree* which is optimized for clique bifiltrations. In this work, we have not run experiments with *2pac*. While it is possible that using the code from [2] together with *2pac* would lead to significant performance gains, for low-dimensional point clouds this seems unlikely to make the performance of $\mathcal{R}_\bullet(\gamma)$ competitive with $\mathcal{I}_\bullet(\gamma)$.

Data Set	#Points	codensity-Rips bifiltration preprocessing with filtration-domination					codensity-Delaunay bifiltration		
		# Edges before	# Edges after	Complex Size	Time	Memory	Complex Size	Time	Memory
S^1	500	124750	15124	10293094	16.24	2573.28	11269	0.02	6.78
	1000	499500	44219	86436503	137.04	21778.87	23611	0.06	9.82
S^2	500	124750	50342	188414574	246.45	47241.98	67763	0.13	19.49
	1000	499500	173725	∞	∞	∞	150747	0.32	38.17
$[0, 1]^2$	500	124750	5922	136392	2.36	37.09	11321	0.03	7.89
	1000	499500	17521	965123	16.76	242.81	23497	0.08	12.8
$[0, 1]^3$	500	124750	10717	1134028	3.55	281.9	70975	0.17	20.65
	1000	499500	43310	20634286	46.91	5200.04	159887	0.36	40.43
$S^1 \times S^1$	500	124750	16665	2775487	5.45	689.69	73967	0.14	21.09
	1000	499500	65558	46094578	73.07	11486.7	171105	0.36	43.69

TABLE 3. Running time (in seconds) and memory consumption (in MB) of minimal presentation computation in homology degree 1. The symbol ∞ means the pipeline ran out of memory and the computation could not finish.

Further experiments. We summarize more experimental findings. The details are in Appendix B.

Subroutines: We measured the performance of the major substeps of our bifiltration algorithm. It turns out that only around 1/6 of the runtime is required to construct the incremental Delaunay complex, around 1/3 for computing the minimum enclosing ball radii, and 1/2 for creating the chain complex structure that we output.

Higher dimensions: Our software is not limited to points clouds in 2 and 3 dimensions. We ran some experiments for higher dimensional data. Not surprisingly, complex size, time, and memory increase significantly when the ambient dimension increases. However, the ratio between the Delaunay triangulation and our incremental construction remains quite small (≤ 10) in the instances we tested.

⁷<https://gitlab.com/flenzen/2-parameter-persistent-cohomology>

Compression: Given the chain complex of a sublevel Delaunay bifiltration, the software *multi-chunk*⁸ [45, 46], computes an algebraically equivalent chain complex whose size is substantially smaller—by up to a factor of 30, in our experiments.

5. CONCLUSION

We have introduced the Delaunay-Čech bifiltration $\mathcal{DC}_\bullet(\gamma)$ of a function γ on a Euclidean point cloud. We have seen that

- (i) $\mathcal{DC}_\bullet(\gamma)$ is topologically well behaved, in the sense that it is equivalent to the offset bifiltration,
- (ii) $\mathcal{DC}_\bullet(\gamma)$ is reasonably small, both in theory and in practice, and
- (iii) for low-dimensional data, $\mathcal{DC}_\bullet(\gamma)$ is far more computable than any known alternative.

Our construction enables bipersistence analysis of tens of thousands of points in low dimensions. Since such data is common in applications and is already actively studied using 2-parameter persistence [51, 71, 8], we foresee our algorithm and its implementation having an immediate practical impact. In fact, for Lipschitz functions γ , it should be possible to handle far bigger data sets by subsampling, at the cost of some small approximation error in the interleaving distance [58].

We have also introduced a second, topologically equivalent bifiltration, the sublevel Delaunay bifiltration $\mathcal{D}_\bullet(\gamma)$, a sub-bifiltration of $\mathcal{DC}_\bullet(\gamma)$ differing only in the radii at which simplices appear. It is natural to ask which radii are faster to compute. For $\mathcal{DC}_\bullet(\gamma)$, the birth radii are obtained via minimum enclosing ball computations, for which high-quality code is available. It is also possible to compute the birth radii for $\mathcal{D}_\bullet(\gamma)$ in constant time per simplex, by extending the usual approach to computing birth radii for the 1-parameter Delaunay filtration [14, Chapter 6.1.2]; the details will be given in a future version of this paper. As we have not implemented this, it is unclear which approach would be faster in practice. It may also be that we can speed up our computations of $\mathcal{DC}_\bullet(\gamma)$ by using a specialized algorithm to compute minimum enclosing balls.

We believe that Delaunay triangulations could be useful for multiparameter persistence in ways that extend well beyond our work. A natural first question is how to extend our approach to the case of multiple functions $\gamma_1, \dots, \gamma_m : X \rightarrow \mathbb{R}$. A solution could be useful in the study of dynamic point processes, which can be modeled using a pair of functions tracking the entrance and removal time of points. A similar problem is to identify a Delaunay variant of the *degree-Rips bifiltration*, an actively studied density-sensitive bifiltration whose definition requires no choice of bandwidth parameter [59, 12, 66].

Acknowledgements. We thank the anonymous reviewers for their valuable comments and suggestions. ÁJA and MK acknowledge the support of the Austrian Science Fund (FWF) grant P 33765-N. ML was supported by a grant from the Simons Foundation (Award ID 963845). MK and ML acknowledge the Dagstuhl Seminar 23192 “Topological Data Analysis and Applications” that initiated this collaboration.

APPENDIX A. PROOF OF THEOREM 3.3

We briefly recall the concepts from discrete Morse theory [44, 30] needed for our argument: A *(discrete) vector field* V on an abstract simplicial complex K is a partition of a subset of K into pairs (σ, τ) with σ a facet of τ . Consider the Hasse diagram of K as an acyclic

⁸Available at https://bitbucket.org/mkerber/multi_chunk/src/master/

directed graph G with edges pointing from smaller to larger faces. Formally, each element of V is an edge in G . If the graph obtained from G by reversing the direction of all edges in V is acyclic, then we call V a *gradient*.

We are interested in gradients because of the following collapsing theorem [44]:

Theorem A.1. *For simplicial complexes $K' \subset K$, if there is a gradient V on K such that $K \setminus K'$ is the union of the pairs of V , then $K \searrow K'$.*

We omit the easy proofs of the following two lemmas:

Lemma A.2. *For simplicial complexes $K' \subset K$, let V be a gradient on K , and let V' be a vector field on K' such that each pair in V' is also in V . Then V' is a gradient on K' .*

Lemma A.3 ([5, Lemma 5.1]). *Let V be a vector field on a simplicial complex K , and fix a vertex x of K . If all pairs of V are of the form $(\sigma, \sigma \cup \{x\})$, then V is a gradient.*

To prove Theorem 3.3, we will use the language of *selective Delaunay complexes* from [5]. Given a subset E of a finite point set $Y \subset \mathbb{R}^d$, the selective Delaunay complex $\mathcal{D}(Y, E)$ consists of all simplices $\sigma \subset Y$ for which there exists a $(d-1)$ -sphere S such that

- (i) all points of σ lie on or inside S and
- (ii) no point of E lies inside S .

For $\sigma \in \mathcal{D}(Y, E)$, let $\rho(\sigma, E)$ denote the minimum radius of such S , and let

$$\mathcal{D}_r(Y, E) = \{\sigma \in \mathcal{D}(Y, E) \mid \rho(\sigma, E) \leq r\}.$$

Note that $\mathcal{D}_r(Y, \emptyset) = \mathcal{C}_r(Y)$, and that if $E \subset F \subset Y$, then $\mathcal{D}_r(Y, F) \subset \mathcal{D}_r(Y, E)$. The sublevel Delaunay bifiltration $\mathcal{D}_\bullet(\gamma)$ can be described in terms of selective Delaunay complexes, as follows: A subset $\sigma \subset X$ with $x_k := \max \sigma$ is a simplex in $\mathcal{D}_{r,s}(\gamma)$ if and only if $\gamma(x_k) \leq s$ and $\sigma \in \mathcal{D}_r(X_k, X_{k-1})$. In particular, if $\sigma \in \mathcal{I}(X)$, then $\rho_\sigma = \rho(\sigma, X_{k-1})$.

As in [5], for $\sigma \subset X$ and $x \in X$, we let $\sigma - x$ and $\sigma + x$ denote the sets $\sigma \setminus \{x\}$ and $\sigma \cup \{x\}$, respectively. Note that one of the sets $\sigma - x$, $\sigma + x$ is equal to σ .

From sublevel Čech to sublevel Delaunay. We first prove the following:

Theorem A.4. *For any $a \in [0, \infty) \times \mathbb{R}$, $\mathcal{C}_a(\gamma) \searrow \mathcal{D}_a(\gamma)$.*

Writing $a = (r, s)$, let $j = \max \{i \mid \gamma(x_i) \leq s\}$. For $i \in \{0, \dots, j\}$, let $\mathcal{U}_i = \mathcal{D}_r(X_j, X_i) \cup \mathcal{D}_a(\gamma)$, where we adopt the convention that $X_0 = \emptyset$. Note that we have a filtration

$$\mathcal{D}_a(\gamma) = \mathcal{U}_j \subset \mathcal{U}_{j-1} \subset \dots \subset \mathcal{U}_0 = \mathcal{C}_a(\gamma).$$

To prove Theorem A.4, it suffices to show that $\mathcal{U}_{i-1} \searrow \mathcal{U}_i$ for each $i \in \{1, \dots, j\}$. We will use the next lemma, which follows immediately from [5, Lemma 5.5] and [5, Lemma 5.7].

Lemma A.5. *For $i \in \{1, \dots, j\}$ and $\sigma \in \mathcal{D}_r(X_j, X_{i-1}) \setminus \mathcal{D}_r(X_j, X_i)$, we also have $\sigma \pm x_i \in \mathcal{D}_r(X_j, X_{i-1}) \setminus \mathcal{D}_r(X_j, X_i)$.*

This implies the analogous statement for the complexes \mathcal{U}_i :

Lemma A.6. *For $i \in \{1, \dots, j\}$ and $\sigma \in \mathcal{U}_{i-1} \setminus \mathcal{U}_i$, we have $\sigma \pm x_i \in \mathcal{U}_{i-1} \setminus \mathcal{U}_i$.*

Proof. We need to show that if $\sigma \in \mathcal{D}_r(X_j, X_{i-1}) \setminus \mathcal{D}_r(X_j, X_i)$ and $\sigma \notin \mathcal{D}_a(\gamma)$, then the same holds for $\sigma \pm x_i$. Lemma A.5 gives that $\sigma \pm x_i \in \mathcal{D}_r(X_j, X_{i-1}) \setminus \mathcal{D}_r(X_j, X_i)$, so it remains only to show that $\sigma \pm x_i \notin \mathcal{D}_a(\gamma)$. Let $x_k := \max \sigma$. We claim that $x_k > x_i$. Suppose to the contrary that $x_k \leq x_i$. Then $X_{k-1} \subset X_{i-1}$ and since $\sigma \in \mathcal{D}_r(X_k, X_{i-1})$, it follows

that $\sigma \in \mathcal{D}_r(X_k, X_{k-1})$. But $\mathcal{D}_r(X_k, X_{k-1}) \subset \mathcal{D}_a(\gamma)$, so $\sigma \in \mathcal{D}_a(\gamma)$, a contradiction. We conclude that $x_k > x_i$ and $\max(\sigma \pm x_i) = x_k$. Since $\sigma \pm x_i \notin \mathcal{D}_r(X_j, X_i)$, we also have $\sigma \pm x_i \notin \mathcal{D}_r(X_k, X_{k-1})$, and consequently, $\sigma \pm x_i \notin \mathcal{D}_a(\gamma)$. \square

Proof of Theorem A.4. For each $i \in \{1, \dots, j\}$, Lemma A.6 gives a partition of $\mathcal{U}_{i-1} \setminus \mathcal{U}_i$ into pairs of the form $(\sigma - x_i, \sigma + x_i)$. By Lemma A.3, this is a gradient. Theorem A.1 now implies that $\mathcal{U}_{i-1} \searrow \mathcal{U}_i$. \square

From sublevel Delaunay-Čech to sublevel Delaunay. The following finishes the proof of Theorem 3.3:

Theorem A.7. *For any $a \in [0, \infty) \times \mathbb{R}$, $\mathcal{DC}_a(\gamma) \searrow \mathcal{D}_a(\gamma)$.*

For $i \in \{1, \dots, |X|\}$, let

$$\begin{aligned} X_{\leq i} &= \{\sigma \subset X \mid \max \sigma \leq x_i\}, \\ X_{=i} &= \{\sigma \subset X \mid \max \sigma = x_i\}, \\ X_{>i} &= \{\sigma \subset X \mid \max \sigma > x_i\}. \end{aligned}$$

Let $X_{\leq 0} = X_{=0} = \emptyset$ and $X_{>0} = X$. For $i \in \{0, \dots, |X|\}$, define the simplicial complex

$$M_i = (X_{>i} \cap \mathcal{D}_a(\gamma)) \cup (X_{\leq i} \cap \mathcal{DC}_a(\gamma)),$$

which is indeed simplicial because, for $\sigma \subset \sigma' \in \mathcal{D}_a(\gamma)$, we have $r_\sigma \leq \rho_\sigma \leq \rho_{\sigma'}$. As before, write $a = (r, s)$ and let $j = \max\{i \mid \gamma(x_i) \leq s\}$. Note that we have a filtration

$$\mathcal{D}_a(\gamma) = M_0 \subset M_1 \subset \dots \subset M_{j-1} \subset M_j = \mathcal{DC}_a(\gamma).$$

As above, to prove Theorem A.7, it suffices to show that $M_i \searrow M_{i-1}$ for each $i \in \{1, \dots, j\}$. We use the following result from [5] about selective Delaunay complexes.

Proposition A.8. *For any $i \in \{1, \dots, |X|\}$, there is a gradient V_i on $\mathcal{C}_r(X_i) \cap \mathcal{D}(X_i, X_{i-1})$ that induces a collapse to $\mathcal{D}_r(X_i, X_{i-1})$, and whose pairs $(\sigma, \sigma + x)$ satisfy $x < x_i$.*

Proof. The vector field V_i is defined by [5, Equation 30 and Lemma 5.6]; it is shown in the proof of [5, Theorem 5.9] that V_i is indeed a gradient. \square

Proof of Theorem A.7. Note that

$$M_i \setminus M_{i-1} = X_{=i} \cap (\mathcal{DC}_a(\gamma) \setminus \mathcal{D}_a(\gamma)).$$

Thus, for a simplex $\sigma \in \mathcal{DC}_a(\gamma)$, we have $\sigma \in M_i \setminus M_{i-1}$ if and only if $\max \sigma = x_i$ and $r_\sigma \leq r < \rho_\sigma$. It follows that $M_i \setminus M_{i-1} = X_{=i} \cap N_i$, where

$$N_i := \mathcal{C}_r(X_i) \cap (\mathcal{D}(X_i, X_{i-1}) \setminus \mathcal{D}_r(X_i, X_{i-1})).$$

V_i partitions N_i into pairs of the form $(\sigma, \sigma + x)$ with $x < x_i$, so if $\sigma \in X_{=i}$, then $\sigma + x \in X_{=i}$. Thus, V_i restricts to a partition of $X_{=i} \cap N_i$, which is a gradient on M_i by Lemma A.2. Theorem A.1 now yields the desired collapse. \square

APPENDIX B. FURTHER EXPERIMENTAL EVALUATION

Full evaluation of size and performance. We enlist the comprehensive results from our experimental runs in Tables 4 and 5.

Sample	#Points	Delaunay size	Random		Density		Height		Eccentricity	
			Size	Ratio	Size	Ratio	Size	Ratio	Size	Ratio
$[0, 1]^2$	1000	5971	19223	3.22	23497	3.94	28167	4.72	34807	5.83
	2000	11971	39801	3.32	48605	4.06	62815	5.25	74391	6.21
	4000	23969	78859	3.29	99339	4.14	138341	5.77	155301	6.48
	8000	47963	158443	3.3	201929	4.21	304331	6.35	326321	6.8
	16000	95951	319753	3.33	410575	4.28	660215	6.88	682773	7.12
	32000	191959	639235	3.33	838631	4.37	1430915	7.45	1408505	7.34
$[0, 1]^3$	1000	27609	122177	4.43	159887	5.79	198433	7.19	244257	8.85
	2000	56299	255927	4.55	345469	6.14	458447	8.14	551599	9.8
	4000	113975	529063	4.64	731093	6.41	1050155	9.21	1193795	10.47
	8000	227809	1070993	4.7	1518117	6.66	2376689	10.43	2562581	11.25
	16000	458947	2172081	4.73	3166425	6.9	5281167	11.51	5418085	11.81
	32000	921399	4359419	4.73	6607583	7.17	11650367	12.64	11290949	12.25
S^1	1000	5975	19481	3.26	23611	3.95	25575	4.28	39419	6.6
	2000	11971	39131	3.27	49593	4.14	57019	4.76	83209	6.95
	4000	23959	79839	3.33	102307	4.27	127111	5.31	180307	7.53
	8000	47967	158789	3.31	209099	4.36	282055	5.88	375891	7.84
	16000	95953	318919	3.32	430991	4.49	619561	6.46	788465	8.22
	32000	191943	638553	3.33	889599	4.63	1343567	7.0	1638579	8.54
S^2	1000	26439	116635	4.41	150747	5.7	175995	6.66	263183	9.95
	2000	54327	245651	4.52	325791	6.0	415555	7.65	600589	11.06
	4000	109987	503831	4.58	709303	6.45	962039	8.75	1347043	12.25
	8000	222339	1040769	4.68	1534939	6.9	2165395	9.74	2984415	13.42
	16000	450133	2104495	4.68	3241029	7.2	4850005	10.77	6380329	14.17
	32000	909567	4266411	4.69	6824453	7.5	10761403	11.83	13738989	15.1
$S^1 \times S^1$	1000	27003	122181	4.52	171105	6.34	230075	8.52	215815	7.99
	2000	52717	257129	4.88	361151	6.85	515437	9.78	467803	8.87
	4000	105249	512521	4.87	747617	7.1	1159641	11.02	937369	8.91
	8000	211885	1010347	4.77	1526509	7.2	2561545	12.09	1911169	9.02
	16000	426531	2028761	4.76	3093869	7.25	5578187	13.08	3912707	9.17
	32000	862789	4065635	4.71	6376129	7.39	12145149	14.08	8118607	9.41

TABLE 4. Size comparison of incremental Delaunay complexes for various datasets (full version of Table 1).

Detailed runtime analysis. We measured the main sub-steps of the computation. There are three steps with significant running time, and we display their contribution to the runtime in Table 6: the time to construct the incremental Delaunay complex, the time to compute all meb radii, and the time to generate the chain complex out of the simplicial complex. The last step is not trivial because computing the boundary maps requires a switch from representing simplices by their boundary vertices (as done in the Simplex tree implementation of GUDHI) to representing simplices by their faces in codimension 1. We observe in Table 6 that this step typically requires around half of the running time. We speculate that a different data structure for simplicial complexes, more suitable for our application, could improve the running time further.

We further see that the computation of minimum enclosing ball radii takes generally more time than constructing the complex itself. We point out here that the tools to compute mebs are not optimized for our application scenario, where the number of points is only slightly

Sample	#Points	Random			Density			Height			Eccentricity		
		Time (s)	Time/simplex (ms)	Memory (GB)	Time (s)	Time/simplex (ms)	Memory (MB)	Time (s)	Time/simplex (ms)	Memory (MB)	Time (s)	Time/simplex (ms)	Memory (MB)
$[0, 1]^2$	1000	0.03	1.74	8.57	0.04	1.9	9.38	0.04	1.52	10.72	0.05	1.39	12.3
	2000	0.08	2.02	13.18	0.08	1.55	14.95	0.1	1.64	18.3	0.12	1.66	20.91
	4000	0.13	1.7	21.73	0.16	1.63	25.94	0.21	1.53	35.36	0.25	1.64	38.74
	8000	0.28	1.79	39.18	0.36	1.76	48.2	0.47	1.55	73.05	0.54	1.65	76.29
	16000	0.67	2.09	74.78	0.83	2.03	93.82	1.13	1.7	155.48	1.21	1.77	156.41
	32000	1.53	2.39	147.96	1.79	2.13	187.54	2.55	1.78	322.46	2.64	1.88	322.64
$[0, 1]^3$	1000	0.25	2.04	31.75	0.28	1.77	40.07	0.34	1.73	50.43	0.45	1.84	60.09
	2000	0.52	2.05	62.64	0.73	2.12	81.86	0.89	1.95	110.41	1.11	2.02	128.71
	4000	1.2	2.28	128.02	1.61	2.21	170.88	2.16	2.05	247.88	2.55	2.14	272.34
	8000	2.63	2.46	246.07	3.49	2.3	342.96	5.1	2.14	554.64	5.64	2.2	586.6
	16000	5.8	2.67	517.54	7.82	2.47	727.03	11.74	2.22	1166.0	12.49	2.31	1196.14
	32000	12.36	2.84	1005.29	16.79	2.54	1505.86	27.07	2.32	2688.1	27.07	2.4	2576.14
S^1	1000	0.03	1.58	8.44	0.05	2.01	9.4	0.04	1.5	9.72	0.05	1.35	13.12
	2000	0.06	1.62	12.87	0.08	1.54	15.08	0.08	1.33	17.14	0.14	1.67	22.79
	4000	0.13	1.69	21.88	0.16	1.58	26.48	0.17	1.36	32.86	0.3	1.66	44.19
	8000	0.28	1.78	39.56	0.35	1.68	50.13	0.44	1.55	68.38	0.64	1.71	87.75
	16000	0.64	2.02	74.72	0.81	1.87	98.46	1.03	1.66	146.57	1.44	1.82	178.85
	32000	1.5	2.35	147.81	1.79	2.01	199.02	2.37	1.76	311.03	3.17	1.94	371.64
S^2	1000	0.21	1.76	30.85	0.26	1.74	37.81	0.33	1.86	44.09	0.47	1.8	63.72
	2000	0.48	1.93	59.57	0.67	2.07	77.06	0.79	1.89	101.46	1.25	2.09	139.36
	4000	1.11	2.2	118.37	1.54	2.16	163.22	1.94	2.02	225.22	3.0	2.23	309.19
	8000	2.5	2.4	244.05	3.57	2.33	354.23	4.57	2.11	496.82	6.95	2.33	681.24
	16000	5.49	2.61	487.78	8.02	2.48	741.83	10.56	2.18	1093.43	15.6	2.44	1501.82
	32000	12.0	2.81	964.62	17.56	2.57	1580.05	24.68	2.29	2469.64	34.62	2.52	3160.35
$S^1 \times S^1$	1000	0.21	1.73	31.89	0.3	1.77	43.03	0.41	1.79	57.21	0.38	1.76	53.09
	2000	0.49	1.92	62.76	0.75	2.06	85.69	1.05	2.03	125.26	0.95	2.04	110.82
	4000	1.11	2.17	122.72	1.59	2.12	170.57	2.44	2.1	265.98	1.98	2.11	224.83
	8000	2.36	2.34	236.03	3.49	2.29	354.77	5.54	2.16	619.1	4.17	2.18	437.08
	16000	5.11	2.52	455.98	7.41	2.4	710.66	12.7	2.28	1271.56	8.94	2.28	910.05
	32000	11.1	2.73	929.58	15.65	2.45	1461.12	28.5	2.35	2796.81	19.08	2.35	1847.01

TABLE 5. Running time (in seconds), the average number of simplices processed per second, and the memory consumption (in MB) for computing the sublevel Delaunay bifiltration (full version of Table 2).

larger than the dimension. There might also be room for improvement here using a different computation method.

Sample	Function	#Points	Overall	Complex	meb	chain complex
$[0, 1]^2$	density	1000	0.04	23.01%	29.67%	37.57%
		2000	0.08	15.59%	35.24%	43.44%
		4000	0.16	16.44%	33.82%	44.58%
		8000	0.36	16.12%	33.29%	45.28%
		16000	0.83	18.54%	31.85%	43.61%
		32000	1.79	18.16%	31.34%	45.11%
S^2	eccentricity	1000	0.47	12.81%	35.02%	50.99%
		2000	1.25	13.57%	33.94%	49.05%
		4000	3.0	11.90%	33.47%	51.07%
		8000	6.95	11.01%	32.66%	52.78%
		16000	15.6	11.03%	31.50%	53.81%
		32000	34.62	11.09%	31.14%	54.12%
$S^1 \times S^1$	random	1000	0.21	13.89%	34.83%	49.76%
		2000	0.49	13.19%	34.06%	50.01%
		4000	1.11	12.17%	33.90%	49.84%
		8000	2.36	12.07%	33.67%	50.50%
		16000	5.11	12.20%	32.96%	50.91%
		32000	11.1	12.09%	33.22%	50.72%

TABLE 6. The time breakdown (in seconds) for computing the sublevel Delaunay bifiltration.

Higher dimensions. Our code can handle point clouds in all dimensions. We display the effect of higher dimensionality in Table 7. We observe that the size increases significantly when increasing the dimension which is expected since the worst-case bound has an exponential dependence on d . However, we observe that the size of the Delaunay triangulation grows at a similar speed, hence the overhead imposed by taking the function γ into account is still relatively small.

Sample	Function	Dim	Size	Time	Memory	Delaunay size	Ratio
$[0, 1]^d$, $n=500$	density	2	10917	0.02	6.58	2977	3.67
		3	70335	0.13	20.48	13505	5.21
		4	463649	1.11	109.95	77747	5.96
		5	3134645	10.36	1575.41	503747	6.22
		6	20632741	78.45	10246.52	3429063	6.02
S^3 , $n=500$	height	4	503865	1.14	121.46	74429	6.77
		5	2417037	7.44	1102.71	319589	7.56
		6	16089733	113.62	7379.98	1699797	9.47
$S^1 \times S^1$, $n=500$	random	3	61847	0.13	18.5	13471	4.59
		4	275805	0.65	67.02	60121	4.59
		5	1602905	5.53	773.18	301171	5.32
		6	7980373	31.01	3971.36	1499809	5.32

TABLE 7. The size of the sublevel Delaunay bifiltration, the running time (in seconds) and memory consumption (in MB). Furthermore, the size of the Delaunay triangulation and the ratio of the sizes are displayed.

Compression. While not exploding in size for low dimension, the sublevel Delaunay bifiltration is still large in size which poses a challenge to subsequent analysis algorithms on such a bifiltration. Recall that we encode the bifiltration as a chain complex, where the chain group in dimension k has the k -simplices of the incremental Delaunay complex as basis. The *multi-chunk* algorithm⁹ [45, 46] replaces a chain complex with a smaller chain complex (whose basis elements no longer correspond to simplices) that is homotopy-equivalent. That is, as long as only topological properties of the bifiltration (such as homology) are subsequently studied, we can post-process with the multi-chunk algorithm to compress the resulting chain complex.

Table 8 shows the results of this post-processing step. We can see the multi-chunk significantly reduces the data size. Depending on the example, the compression rate was between 0.0297 and 0.593. The running time of multi-chunk varies a lot from instance to instance; this has to do with the special topological configuration of the sublevel sets and we omit a detailed explanation. Finally, we can observe that the ratio between the post-processed chain complex and the Delaunay triangulation appears to be non-increasing in many cases. This brings the question whether it is possible to compute the compressed version of the sublevel Delaunay bifiltration directly, without computing the uncompressed version first. Such an algorithm could potentially scale linearly in practice, just like the computation of the Delaunay computation.

⁹Available at https://bitbucket.org/mkerber/multi_chunk/src/master/

Sample	Function	#Points	Complex		Multi-chunk		Delaunay size	Ratio	
			Size	Time	Size	Compression			Time
$[0, 1]^2$	random	1000	19223	0.0	10979	0.57	0.0	5971	1.84
		2000	39801	0.01	22385	0.56	0.01	11971	1.87
		4000	78859	0.02	45381	0.58	0.01	23969	1.89
		8000	158443	0.05	92339	0.58	0.03	47963	1.92
		16000	319753	0.11	187871	0.59	0.08	95951	1.96
		32000	639235	0.28	376459	0.59	0.14	191959	1.96
S^2	density	1000	150747	0.04	14223	0.09	0.02	26439	0.54
		2000	325791	0.1	29503	0.09	0.06	54327	0.54
		4000	709303	0.18	62039	0.09	0.24	109987	0.56
		8000	1534939	0.46	127949	0.08	0.86	222339	0.58
		16000	3241029	0.92	268187	0.08	3.17	450133	0.6
		32000	6824453	2.06	557371	0.08	10.62	909567	0.61
$S^1 \times S^1$	height	1000	230075	0.05	10793	0.05	0.03	27003	0.4
		2000	515437	0.12	21305	0.04	0.05	52717	0.4
		4000	1159641	0.29	40501	0.03	0.14	105249	0.38
		8000	2561545	0.65	81615	0.03	0.34	211885	0.39
		16000	5578187	1.41	167225	0.03	0.78	426531	0.39
		32000	12145149	3.15	357835	0.03	1.66	862789	0.41

TABLE 8. The size of the sublevel Delaunay bifiltration, the running time (in seconds) and memory consumption (in MB). Furthermore, the size of the Delaunay triangulation and the ratio of the sizes are displayed.

REFERENCES

- [1] Aaron Adcock, Daniel Rubin, and Gunnar Carlsson. Classification of hepatic lesions using the matching metric. *Computer vision and image understanding*, 121:36–42, 2014. doi:10.1016/j.cviu.2013.10.014.
- [2] Ángel Javier Alonso, Michael Kerber, and Siddharth Pritam. Filtration-domination in bifiltered graphs. In *2023 Proceedings of the Symposium on Algorithm Engineering and Experiments (ALENEX)*, pages 27–38. SIAM, 2023.
- [3] Hideto Asashiba, Emerson G. Escolar, Ken Nakashima, and Michio Yoshiwaki. On approximation of 2d persistence modules by interval-decomposables. *Journal of Computational Algebra*, 6-7:100007, 2023. doi:10.1016/j.jaca.2023.100007.
- [4] Ulrich Bauer. Ripser: efficient computation of Vietoris-Rips persistence barcodes. *Journal of Applied and Computational Topology*, 5(3):391–423, 2021. doi:10.1007/s41468-021-00071-5.
- [5] Ulrich Bauer and Herbert Edelsbrunner. The Morse theory of Čech and Delaunay complexes. *Transactions of the American Mathematical Society*, 369(5):3741–3762, 2017. doi:10.1090/tran/6991.
- [6] Ulrich Bauer, Michael Kerber, Fabian Roll, and Alexander Rolle. A unified view on the functorial nerve theorem and its variations. *Expositiones Mathematicae*, 41(4):125503, 2023. doi:10.1016/j.exmath.2023.04.005.
- [7] Ulrich Bauer, Fabian Lenzen, and Michael Lesnick. Efficient Two-Parameter Persistence Computation via Cohomology. In *39th International Symposium on Computational Geometry (SoCG 2023)*. doi:10.4230/LIPIcs.SoCG.2023.15.
- [8] Katherine Benjamin, Aneesha Bhandari, Zhouchun Shang, Yanan Xing, Yanru An, Nannan Zhang, Yong Hou, Ulrike Tillmann, Katherine R. Bull, and Heather A. Harrington. Multiscale topology classifies and quantifies cell types in subcellular spatial transcriptomics, 2022. arXiv:2212.06505.
- [9] Ranita Biswas, Sebastiano Cultrera di Montesano, Ondřej Draganov, Herbert Edelsbrunner, and Morteza Saghafian. On the size of chromatic Delaunay mosaics, 2022. arXiv:2212.03121.
- [10] Håvard Bakke Bjerkevik and Michael Lesnick. ℓ^p -distances on multiparameter persistence modules, 2021. arXiv:2106.13589.
- [11] Benjamin Blanchette, Thomas Brüstle, and Eric J. Hanson. Homological approximations in persistence theory. *Canadian Journal of Mathematics*, pages 1–38, 2022. doi:10.4153/s0008414x22000657.
- [12] Andrew J. Blumberg and Michael Lesnick. Stability of 2-parameter persistent homology. *Foundations of Computational Mathematics*. doi:10.1007/s10208-022-09576-6.

- [13] Andrew J. Blumberg and Michael Lesnick. Universality of the homotopy interleaving distance. *Transactions of the American Mathematical Society*, in press. [arXiv:1705.01690](#).
- [14] Jean-Daniel Boissonnat, Frédéric Chazal, and Mariette Yvinec. *Geometric and topological inference*. Cambridge University Press, 2018. [doi:10.1017/9781108297806](#).
- [15] Jean-Daniel Boissonnat, Olivier Devillers, and Samuel Hornus. Incremental construction of the Delaunay triangulation and the Delaunay graph in medium dimension. In *Proceedings of the Twenty-Fifth Annual Symposium on Computational Geometry*, SCG '09, page 208–216, 2009. [doi:10.1145/1542362.1542403](#).
- [16] Jean-Daniel Boissonnat, Olivier Devillers, Sylvain Pion, Monique Teillaud, and Mariette Yvinec. Triangulations in CGAL. *Computational Geometry. Theory and Applications*, 22(1-3):5–19, 2002. [doi:10.1016/S0925-7721\(01\)00054-2](#).
- [17] Jean-Daniel Boissonnat and Clément Maria. The simplex tree: An efficient data structure for general simplicial complexes. *Algorithmica*, 70(3):406–427, 2014. [doi:10.1007/s00453-014-9887-3](#).
- [18] Jean-Daniel Boissonnat and Siddharth Pritam. Edge collapse and persistence of flag complexes. In *36th International Symposium on Computational Geometry (SoCG 2020)*. [doi:10.4230/LIPIcs.SoCG.2020.19](#).
- [19] Jean-Daniel Boissonnat and Monique Teillaud. On the randomized construction of the Delaunay tree. *Theoretical Computer Science*, 112(2):339–354, 1993. [doi:10.1016/0304-3975\(93\)90024-N](#).
- [20] Magnus Bakke Botnan and Michael Lesnick. An introduction to multiparameter persistence. *Proceedings of the 2020 International Conference on Representations of Algebras*, in press. [arXiv:2203.14289](#).
- [21] Magnus Bakke Botnan, Steffen Oppermann, and Steve Oudot. Signed Barcodes for Multi-Parameter Persistence via Rank Decompositions. In *38th International Symposium on Computational Geometry (SoCG 2022)*. [doi:10.4230/LIPIcs.SoCG.2022.19](#).
- [22] Magnus Bakke Botnan, Steffen Oppermann, Steve Oudot, and Luis Scoccola. On the bottleneck stability of rank decompositions of multi-parameter persistence modules, 2022. [arXiv:2208.00300](#).
- [23] Adrian Bowyer. Computing Dirichlet tessellations. *The Computer Journal*, 24(2):162–166, 1981. [doi:10.1093/comjnl/24.2.162](#).
- [24] Chen Cai, Woojin Kim, Facundo Mémoli, and Yusu Wang. Elder-rule-staircodes for augmented metric spaces. *SIAM Journal on Applied Algebra and Geometry*, 5(3):417–454, 2021. [doi:10.1137/20M1353605](#).
- [25] Zixuan Cang, Lin Mu, and Guo-Wei Wei. Representability of algebraic topology for biomolecules in machine learning based scoring and virtual screening. *PLoS computational biology*, 14(1):e1005929, 2018. [doi:10.1371/journal.pcbi.1005929](#).
- [26] Zixuan Cang and Guo-Wei Wei. Persistent cohomology for data with multicomponent heterogeneous information. *SIAM Journal on Mathematics of Data Science*, 2(2):396–418, 2020. [doi:10.1137/19M1272226](#).
- [27] Gunnar Carlsson, Tigran Ishkhanov, Vin De Silva, and Afra Zomorodian. On the local behavior of spaces of natural images. *International Journal of Computer Vision*, 76(1):1–12, 2008. [doi:10.1007/s11263-007-0056-x](#).
- [28] Gunnar Carlsson and Afra Zomorodian. The theory of multidimensional persistence. *Discrete & Computational Geometry*, 42(1):71–93, 2009. [doi:10.1007/s00454-009-9176-0](#).
- [29] Mathieu Carrière and Andrew Blumberg. Multiparameter persistence images for topological machine learning. In *Conference on Neural Information Processing Systems (NIPS'20)*, page 22432–22444.
- [30] Manoj K. Chari. On discrete Morse functions and combinatorial decompositions. *Discrete Mathematics*, 217(1-3):101–113, 2000. [doi:10.1016/S0012-365X\(99\)00258-7](#).
- [31] René Corbet, Ulderico Fugacci, Michael Kerber, Claudia Landi, and Bei Wang. A kernel for multi-parameter persistent homology. *Computers & Graphics: X*, 2:100005, 2019. [doi:10.1016/j.cagx.2019.100005](#).
- [32] René Corbet, Michael Kerber, Michael Lesnick, and Georg Osang. Computing the multicover bifiltration. *Discrete & Computational Geometry*, 70(2):376–405, 2023. [doi:10.1007/s00454-022-00476-8](#).
- [33] Mark de Berg, Otfried Cheong, Marc J. van Kreveld, and Mark H. Overmars. *Computational geometry: algorithms and applications, 3rd Edition*. Springer, 2008. [doi:10.1007/978-3-540-77974-2](#).
- [34] Olivier Devillers. The Delaunay hierarchy. *International Journal of Foundations of Computer Science*, pages 163–180, 2002. [doi:10.1142/S0129054102001035](#).

- [35] Olivier Devillers, Samuel Hornus, and Clément Jamin. dD triangulations. In *CGAL User and Reference Manual*. CGAL Editorial Board, 5.5.2 edition, 2023. URL: <https://doc.cgal.org/5.5.2/Manual/packages.html#PkgTriangulations>.
- [36] Olivier Devillers, Sylvain Pion, and Monique Teillaud. Walking in a triangulation. *International Journal of Foundations of Computer Science*, 13(02):181–199, 2002. doi:10.1142/S0129054102001047.
- [37] Tamal K. Dey, Woojin Kim, and Facundo Mémoli. Computing Generalized Rank Invariant for 2-Parameter Persistence Modules via Zigzag Persistence and Its Applications. In *38th International Symposium on Computational Geometry (SoCG 2022)*. doi:10.4230/LIPIcs.SoCG.2022.34.
- [38] Sebastiano Cultrera di Montesano, Ondřej Draganov, Herbert Edelsbrunner, and Morteza Saghafian. Persistent homology of chromatic alpha complexes, 2022. arXiv:2212.03128.
- [39] Herbert Edelsbrunner and John L. Harer. *Computational topology: an introduction*. American Mathematical Society, Providence, RI, 2010. doi:10.1090/mbk/069.
- [40] Herbert Edelsbrunner and Georg Osang. The multi-cover persistence of Euclidean balls. *Discrete & Computational Geometry*, 65(4):1296–1313, 2021. doi:10.1007/s00454-021-00281-9.
- [41] Herbert Edelsbrunner and Georg Osang. A simple algorithm for higher-order Delaunay mosaics and alpha shapes. *Algorithmica*, 85(1):277–295, 2023. doi:10.1007/s00453-022-01027-6.
- [42] Herbert Edelsbrunner and Nimish R. Shah. Incremental topological flipping works for regular triangulations. *Algorithmica*, 15(3):223–241, 1996. doi:10.1007/s004539900013.
- [43] Kaspar Fischer, Bernd Gärtner, Thomas Herrmann, Michael Hoffmann, and Sven Schönherr. Bounding volumes. In *CGAL User and Reference Manual*. CGAL Editorial Board, 5.5.2 edition, 2023. URL: <https://doc.cgal.org/5.5.2/Manual/packages.html#PkgBoundingVolumes>.
- [44] Robin Forman. Morse theory for cell complexes. *Advances in Mathematics*, 134(1):90–145, 1998. doi:10.1006/aima.1997.1650.
- [45] Ulderico Fugacci and Michael Kerber. Chunk reduction for multi-parameter persistent homology. In *35th International Symposium on Computational Geometry (SoCG 2019)*. doi:10.4230/LIPIcs.SoCG.2019.37.
- [46] Ulderico Fugacci, Michael Kerber, and Alexander Rolle. Compression for 2-parameter persistent homology. *Computational Geometry*, 109:101940, 2023. doi:10.1016/j.comgeo.2022.101940.
- [47] Bernd Gärtner. Fast and robust smallest enclosing balls. In *Algorithms - ESA '99, 7th Annual European Symposium*. doi:10.1007/3-540-48481-7_29.
- [48] Marc Glisse and Siddharth Pritam. Swap, Shift and Trim to Edge Collapse a Filtration. In *38th International Symposium on Computational Geometry (SoCG 2022)*. doi:10.4230/LIPIcs.SoCG.2022.44.
- [49] Clément Jamin, Sylvain Pion, and Monique Teillaud. 3D triangulations. In *CGAL User and Reference Manual*. CGAL Editorial Board, 5.5.2 edition, 2023. URL: <https://doc.cgal.org/5.5.2/Manual/packages.html#PkgTriangulation3>.
- [50] Heinrich Jung. Ueber die kleinste Kugel, die eine räumliche Figur einschliesst. *Journal für die Reine und Angewandte Mathematik*, 123:241–257, 1901. doi:10.1515/crll.1901.123.241.
- [51] Bryn Keller, Michael Lesnick, and Theodore L Willke. Persistent homology for virtual screening. 2018. doi:10.26434/chemrxiv.6969260.v3.
- [52] Michael Kerber and Michael Lesnick. scc2020: A file format for sparse chain complexes in TDA, 2021. URL: https://bitbucket.org/mkerber/chain_complex_format/.
- [53] Michael Kerber and Arnur Nigmatov. Efficient Approximation of the Matching Distance for 2-Parameter Persistence. In *36th International Symposium on Computational Geometry (SoCG 2020)*. doi:10.4230/LIPIcs.SoCG.2020.53.
- [54] Michael Kerber and Alexander Rolle. Fast minimal presentations of bi-graded persistence modules. In *Proceedings of the Symposium on Algorithm Engineering and Experiments, ALENEX 2021*. doi:10.1137/1.9781611976472.16.
- [55] Woojin Kim and Facundo Mémoli. Generalized persistence diagrams for persistence modules over posets. *Journal of Applied and Computational Topology*, 5(4):533–581, 2021. doi:10.1007/s41468-021-00075-1.
- [56] Edoardo Lanari and Luis Scoccola. Rectification of interleavings and a persistent Whitehead theorem. *Algebraic & Geometric Topology*, 23(2):803–832, 2023. doi:10.2140/agt.2023.23.803.
- [57] Charles L. Lawson. Properties of n -dimensional triangulations. *Computer Aided Geometric Design*, 3(4):231–246 (1987), 1986. doi:10.1016/0167-8396(86)90001-4.

- [58] Michael Lesnick. The theory of the interleaving distance on multidimensional persistence modules. *Foundations of Computational Mathematics*, 15(3):613–650, 2015. doi:10.1007/s10208-015-9255-y.
- [59] Michael Lesnick and Matthew Wright. Interactive visualization of 2-D persistence modules. 2015. arXiv:1512.00180.
- [60] Michael Lesnick and Matthew Wright. Computing minimal presentations and bigraded Betti numbers of 2-parameter persistent homology. *SIAM Journal on Applied Algebra and Geometry*, 6(2):267–298, 2022. doi:10.1137/20M1388425.
- [61] David Loiseaux, Luis Scoccola, Mathieu Carrière, Magnus Bakke Botnan, and Steve Oudot. Stable vectorization of multiparameter persistent homology using signed barcodes as measures. 2023. arXiv:2306.03801.
- [62] Clément Maria. Filtered complexes. In *GUDHI User and Reference Manual*. GUDHI Editorial Board, 2015. URL: http://gudhi.gforge.inria.fr/doc/latest/group__simplex__tree.html.
- [63] Alexander McCleary and Amit Patel. Edit distance and persistence diagrams over lattices. *SIAM Journal on Applied Algebra and Geometry*, 6(2):134–155, 2022. doi:10.1137/20M1373700.
- [64] Dmitriy Morozov and Amit Patel. Output-sensitive computation of generalized persistence diagrams for 2-filtrations. 2021. arXiv:2112.03980.
- [65] Yohai Reani and Omer Bobrowski. A coupled alpha complex. 2021. arXiv:2105.08113.
- [66] Alexander Rolle. The degree-Rips complexes of an annulus with outliers. In *38th International Symposium on Computational Geometry, SoCG 2022*. doi:10.4230/LIPIcs.SoCG.2022.58.
- [67] Vincent Rouvreau and Hind Montassif. Čech complex. In *GUDHI User and Reference Manual*. GUDHI Editorial Board, 3.8.0 edition, 2023. URL: https://gudhi.inria.fr/doc/3.8.0/group__cech__complex.html.
- [68] Luis Scoccola and Alexander Rolle. Persistable: persistent and stable clustering. *Journal of Open Source Software*, 8(83):5022, 2023. doi:10.21105/joss.05022.
- [69] Donald R. Sheehy. A multicover nerve for geometric inference. In *CCCG: Canadian Conference in Computational Geometry*, 2012. URL: <http://2012.cccg.ca/e-proceedings.pdf>.
- [70] Oliver Vipond. Multiparameter persistence landscapes. *Journal of Machine Learning Research*, 21(61):1–38, 2020. URL: <http://jmlr.org/papers/v21/19-054.html>.
- [71] Oliver Vipond, Joshua A. Bull, Philip S. Macklin, Ulrike Tillmann, Christopher W. Pugh, Helen M. Byrne, and Heather A. Harrington. Multiparameter persistent homology landscapes identify immune cell spatial patterns in tumors. *Proceedings of the National Academy of Sciences*, 118(41):e2102166118, 2021. doi:10.1073/pnas.2102166118.
- [72] David F. Watson. Computing the n -dimensional Delaunay tessellation with application to Voronoi polytopes. *The Computer Journal*, 24(2):167–172, 1981. doi:10.1093/comjnl/24.2.167.
- [73] J. H. C. Whitehead. Simplicial Spaces, Nuclei and m -Groups. *Proceedings of the London Mathematical Society. Second Series*, 45(4):243–327, 1939. doi:10.1112/plms/s2-45.1.243.
- [74] Cheng Xin, Soham Mukherjee, Shreyas N. Samaga, and Tamal K. Dey. Gril: A 2-parameter persistence based vectorization for machine learning. 2023. arXiv:2304.04970.
- [75] Mariette Yvinec. 2D triangulations. In *CGAL User and Reference Manual*. CGAL Editorial Board, 5.5.2 edition, 2023. URL: <https://doc.cgal.org/5.5.2/Manual/packages.html#PkgTriangulation2>.

INSTITUTE OF GEOMETRY, GRAZ UNIVERSITY OF TECHNOLOGY, AUSTRIA

Email address: alonsohernandez@tugraz.at

Email address: kerber@tugraz.at

SUNY ALBANY, ALBANY, NY, USA

Email address: tlam@albany.edu

Email address: mlesnick@albany.edu